NJC

Accepted Manuscript

This is an *Accepted Manuscript*, which has been through the Royal Society of Chemistry peer review process and has been accepted for publication.

Accepted Manuscripts are published online shortly after acceptance, before technical editing, formatting and proof reading. Using this free service, authors can make their results available to the community, in citable form, before we publish the edited article. We will replace this *Accepted Manuscript* with the edited and formatted *Advance Article* as soon as it is available.

You can find more information about *Accepted Manuscripts* in the Information for Authors.

Please note that technical editing may introduce minor changes to the text and/or graphics, which may alter content. The journal's standard Terms & Conditions and the Ethical guidelines still apply. In no event shall the Royal Society of Chemistry be held responsible for any errors or omissions in this *Accepted Manuscript* or any consequences arising from the use of any information it contains.

ROYAL SOCIETY OF CHEMISTRY

www.rsc.org/njc

Cite this: DOI: 10.1039/c0xx00000x

www.rsc.org/xxxxxx

ARTICLE TYPE

Tunable and Enhanced Simultaneous Magnetism-Luminescence Bifunctionality Assembled into a Coaxial Nanofiber

Fei Bi, Xiangting Dong*, Jinxian Wang, Guixia Liu

Received (in XXX, XXX) Xth XXXXXXXXX 20XX, Accepted Xth XXXXXXXXX 20XX

DOI: 10.1039/b000000x

[$CoFe_2O_4$/PVP]@[($Y(NO_3)_3$+$Tb(NO_3)_3$+$Al(NO_3)_3$)/PVP] composite coaxial nanofibers have been successfully fabricated via electrospinning technology using a homemade coaxial spinneret. A new structure of $CoFe_2O_4$@YAG:Tb^{3+} magnetic-luminescent bifunctional coaxial nanofibers is obtained by calcination of the prepared electrospun composite coaxial nanofibers. The morphologies, structures, magnetic and luminescent properties of the final products were investigated in detail by X-ray diffractometry (XRD), scanning electron microscopy (SEM), transmission electron microscopy (TEM), fluorescence spectroscopy and vibrating sample magnetometry (VSM). The results show the $CoFe_2O_4$@YAG:7%Tb^{3+} magnetic-luminescent bifunctional coaxial nanofibers simultaneously possess superior magnetic and luminescent properties due to isolation of the YAG:7%Tb^{3+} luminescence center from $CoFe_2O_4$ magnetic nanofibers. Furthermore, the luminescent intensity, color and saturation magnetization of the coaxial nanofibers can be tuned via adjusting the concentrations of rare earth ions and the amount of $CoFe_2O_4$ magnetic nanofibers. The bifunctional magnetic-luminescent $CoFe_2O_4$@YAG:7%Tb^{3+} coaxial nanofibers have potential applications in biomedical area, such as drug-delivery systems, cell labeling and separation, enhancement for magnetic resonance imaging and subsequent optical identification. More importantly, the design conception and construction technology can fit the elaboration of any other bifunctional coaxial nanofiber.

1 Introduction

Nowadays, magnetic-luminescent bifunctional nanomaterials have been proved to be very promising nanomaterials especially in the biomedical field, where they are used as drug-delivery systems, magnetic resonance imaging contrast enhancers and useful tools for cell labeling and separation[1-5]. Another application might be a magnetic field sensor or magnetically manipulated fiber sensor[6]. Most of the magnetic-luminescent nanomaterials are core-shell structures. In general, organic dyes and quantum dot (QDs) have been used as the luminescence shell of the core-shell structured magnetic-luminescent nanomaterials[7-9]. But, the photobleaching and quenching properties of organic dyes and the toxicity of QDs have seriously limited their applications[10]. Compared with organic dyes and QDs, lanthanide-doped nanomaterials have begun to gain attention due to their excellent luminescence properties, especially Tb^{3+}-activated $Y_3Al_5O_{12}$ (YAG) phosphor has luminescence properties fairly insensitive to temperature variation and shows little tendency to saturate at high current excitations. Furthermore, YAG:Tb^{3+} nanomaterials have excellent luminescent properties owing to the f-f electron transition of Tb^{3+} ions, and they have received widespread attention due to their excellent performance[11-14].

Spinel cobalt ferrite ($CoFe_2O_4$) is a type of ferromagnetic materials, which is of importance in the fundamental sciences and technological application. Although $CoFe_2O_4$ nanomaterials have disadvantages, such as the low magnetic energy in per unit volume[15], $CoFe_2O_4$ also has moderate saturation magnetization and excellent physical and chemical stability, which endow $CoFe_2O_4$ nanomaterials suitable for numerous technological applications[16]. $CoFe_2O_4$ has been proposed for biomedical applications since it is known to have large anisotropy compared to other oxide ferrites. As the magnetic anisotropy is directly connected to hyperthermic efficiency, the use of cobalt ferrite can be useful in therapeutic application[17, 18]. Presently, researchers are mainly focused on the preparation, properties and applications of magnetic-luminescent bifunctional nanoparticles owing to the magnetic components of magnetic-luminescent bifunctional nanomaterials would either allow for external manipulation of the carrier with a magnetic field, or use of the carrier for magnetic separation followed by luminescent detection. Nowadays, the one-dimensional (1D) magnetic-luminescent nanomaterials (such as long nanofibers and short nanofibers) can be used in biomedical application. The studies show that these nanomaterials have low toxicity in drug delivery in cells[19, 20]. Therefore, it is an urgent subject to study on the performances and fabrication of new morphologies 1D magnetic-luminescent nanomaterials.

Electrospinning is a simple and versatile technique to process polymers and related materials into one-dimensional structural fibers with controllable compositions, diameters, and

porosities for a variety of applications[21-25]. This method not only has attracted extensive academic investigations, but is also applied in many areas. By now, various one-dimensional (1D) nanomaterials were prepared via electrospinning in literatures[26, 27]. Based on the above studies and previous investigations of magnetic-luminescent bifunctional nanoparticles, it has been proven that the existence of magnetic nanomaterials will greatly decrease the luminescence of rare earth compounds if dark-colored magnetic nanomaterials directly contact with the rare earth luminescent compounds[28-31]. In order to achieve the strong luminescence, rare earth compounds must be effectively isolated from magnetic nanomaterials to avoid direct contacting. The peculiar nanostructure of coaxial nanofibers can help to realize this academic idea. The magnetic nanomaterials are only dispersed in the core of the coaxial nanofibers and rare earth luminescent compounds are merely dispersed in the shell of the coaxial nanofibers, and thus it is expected that the coaxial nanofibers simultaneously exhibit excellent magnetic and luminescent properties.

In this paper, we designed and fabricated magnetic-luminescent bifunctional $CoFe_2O_4$@YAG:Tb^{3+} coaxial nanofibers via electrospinning using a homemade spinneret. This coaxial nanostructure can successfully realize the effective separation of $CoFe_2O_4$ nanofibers from the YAG:Tb^{3+} luminescence center. The structure, morphology, luminescence performances and magnetic properties of the $CoFe_2O_4$@YAG:Tb^{3+} coaxial nanofibers were investigated in detail, and some meaningful results were obtained.

2 Experimental section

2.1 Chemicals

Polyvinyl pyrrolidone (PVP, M_w=1 300 000) and N, N-dimethylformamide (DMF) were purchased from Tianjin Tiantai Fine Chemical Reagents Co., Ltd. HNO_3 was bought from Beijing Chemical Company. Y_2O_3 (99.99%), Tb_4O_7 (99.99%), $Al(NO_3)_3·9H_2O$, $Fe(NO_3)_3·9H_2O$ and $Co(NO_3)_2·6H_2O$ were bought from Sinopharm Chemical Reagent Co., Ltd. All chemicals were of analytical grade and directly used as received without further purification. $Y(NO_3)_3·6H_2O$ and $Tb(NO_3)_3·6H_2O$ were prepared by dissolving Y_2O_3 and Tb_4O_7 in dilute nitric acid, followed by crystallizing from the solution through evaporating the excess water and HNO_3 by heating.

2.2 Preparation of $CoFe_2O_4$ nanofibers

A traditional single-spinneret electrospinning instrument was used to prepare $CoFe_2O_4$ nanofibers (named S). In a typical procedure of preparing spinning solution for fabricating $CoFe_2O_4$ nanofibers, 1 mmol of $Fe(NO_3)_3·9H_2O$, 0.5 mmol of $Co(NO_3)_2·6H_2O$ and 2.2 g of PVP were dissolved into 15.8 g of DMF under continuous stirring. The spinning solution was stirred for 4 h to form homogeneous mixture solutions for next-step electrospinning. Then, the spinning solution was injected into a traditional single-spinneret electrospinning setup, $[Fe(NO_3)_3+Co(NO_3)_2]$/PVP composite nanofibers have been prepared by electrospinning. The electrospinning parameters were as follows: the distance between the spinneret (a plastic needle) and collector was fixed at 18 cm and high voltage power supply was maintained at 15 kV leading to the obtaining of $[Fe(NO_3)_3+Co(NO_3)_2]$/PVP composite nanofibers. The room temperature was 20-24 °C and the relative humidity was 60%-70%. $CoFe_2O_4$ nanofibers (S) can be obtained when the relevant composite nanofibers were annealed in air at 900 °C for 8 h with the heating rate of 1 °C·min^{-1}.

2.3 Fabrication of $CoFe_2O_4$@YAG:7%Tb^{3+} coaxial nanofibers and $CoFe_2O_4$/YAG:7%Tb^{3+} composite nanofibers

In the preparation of the core spinning solution, $CoFe_2O_4$ magnetic nanofibers (S) were ultrasonically dispersed in DMF for 20 min at room temperature, then a certain amount of PVP was added into the above mixture with stirring for 12 h, the final mixture was denoted as the core spinning solution A. The shell spinning solution for preparing $CoFe_2O_4$@YAG:7%Tb^{3+} coaxial nanofibers was prepared as follows: a mixed solution of $Y(NO_3)_3·6H_2O$, $Tb(NO_3)_3·6H_2O$, $Al(NO_3)_3·9H_2O$, PVP and DMF was prepared as the shell spinning solution B, which was stirred for 12 h to form uniform solution for next-step electrospinning. Other series of $CoFe_2O_4$@YAG:x%Tb^{3+} [x=1, 5 and 9, x stands for molar ratio of Tb^{3+} to $(Y^{3+}+Tb^{3+})$] coaxial nanofibers were also prepared by the similar procedure except for different percentage of rare earth nitrates in the shell spinning solution. The compositions and contents of the materials of the core spinning solution A and the shell spinning solution B were shown in Table 1.

$CoFe_2O_4$@YAG:Tb^{3+} coaxial nanofibers were prepared using an electrospinning setup with a homemade coaxial spinneret, as indicated in Figure 1. The core spinning solution was injected into the inner plastic syringe while the shell spinning solution was loaded into the outer one. A piece of flat iron net used as collector was put about 18 cm away from the tip of the coaxial needle to collect the coaxial nanofibers. A positive direct current (DC) voltage of 15 kV was applied between the spinneret and the collector. The electrospinning process was carried out at ambient temperature of 22-24 °C and relative air humidity of 60%-70%.

$[CoFe_2O_4/PVP]@[(Y(NO_3)_3+Tb(NO_3)_3+Al(NO_3)_3)/PVP]$ composite coaxial nanofibers were successfully prepared via the coaxial electrospinning. $CoFe_2O_4$@YAG:x%Tb^{3+} [x=1, 5, 7 and 9] coaxial nanofibers were obtained after annealing the relevant composite coaxial nanofibers in air at 800 °C for 8 h with the heating rate of 1 °C·min^{-1}.

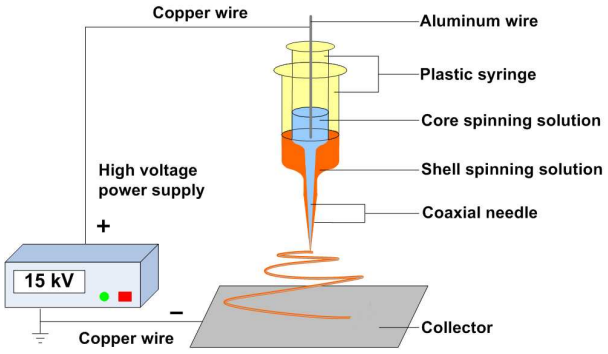

Figure 1. Schematic diagram of electrospinning setup

Meanwhile, $CoFe_2O_4$/YAG:7%Tb^{3+} composite nanofibers (named S_{b1} as shown in Table 1), as a contrast sample, were also prepared to study the superiority of the structure of coaxial nanofibers. $CoFe_2O_4$/YAG:7%Tb^{3+} composite nanofibers were fabricated by mixing the core spinning solution A1

($CoFe_2O_4$/PVP=1:1) and the shell spinning solution B3 (Tb^{3+}/Y^{3+}=7:93) together via using a traditional single-spinneret electrospinning setup, and the spinning parameters were the same as those for the fabrication of the coaxial nanofibers. $CoFe_2O_4$/YAG:7%Tb^{3+} composite nanofibers can be obtained after annealing the relevant composite nanofibers in air at 800 °C for 8 h with the heating rate of 1 °C·min^{-1}.

Table 1. Compositions and contents of the core spinning solution A and the shell spinning solution B

Samples	Spinning solutions	PVP/g	DMF/g	$CoFe_2O_4$ nanofibers (S)/g	Y_2O_3/g	Tb_4O_7/g	$Al(NO_3)_3·9H_2O$/g
S_{a1}	A1 ($CoFe_2O_4$/PVP=1:1)	1.0000	6.6921	1.0000			
	B1 (Tb^{3+}/Y^{3+}=1:99)	1.0707	5.0725		0.0830	0.0014	0.4644
S_{a2}	A1 ($CoFe_2O_4$/PVP=1:1)	1.0000	6.6921	1.0000			
	B2 (Tb^{3+}/Y^{3+}=5:95)	1.0707	5.0720		0.0794	0.0069	0.4630
S_{a3}	A1 ($CoFe_2O_4$/PVP=1:1)	1.0000	6.6921	1.0000			
	B3 (Tb^{3+}/Y^{3+}=7:93)	1.0707	5.0717		0.0776	0.0097	0.4623
S_{a4}	A1 ($CoFe_2O_4$/PVP=1:1)	1.0000	6.6921	1.0000			
	B4 (Tb^{3+}/Y^{3+}=9:91)	1.0707	5.0714		0.0759	0.0124	0.4616
S_{a5}	A2 ($CoFe_2O_4$/PVP=1:3)	3.0000	20.0762	1.0000			
	B3 (Tb^{3+}/Y^{3+}=7:93)	1.0707	5.0717		0.0776	0.0097	0.4623
S_{a6}	A3 ($CoFe_2O_4$/PVP=1:5)	5.0000	33.4600	1.0000			
	B3 (Tb^{3+}/Y^{3+}=7:93)	1.0707	5.0717		0.0776	0.0097	0.4623
S_{b1}	Mixing A1 and B3	2.0707	11.7638	1.0000	0.0776	0.0097	0.4623

2.4 Characterization

The samples were identified by an X-ray powder diffractometer (XRD, Bruker D8 FOCUS) with Cu Kα radiation, and the operation voltage and current were kept at 40 kV and 20 mA, respectively. The morphology and internal structure of samples were observed by a field emission scanning electron microscope (SEM, XL-30) and a transmission electron microscope (TEM, JEM-2010), respectively. The luminescent properties of samples were investigated by a Hitachi fluorescence spectrophotometer F-7000. The magnetic performance of samples was measured by a vibrating sample magnetometer (VSM, MPMS SQUID XL). For magnetic property measurements, 0.03-0.05 g of each sample was loaded into a cylindrical sample cell (sample cell size: 5 mm in diameter, 6 mm in height). The actual quantity of the sample was weighed and then loaded into the VSM operation system. The ultraviolet-visible diffuse reflectance spectrum of the sample was determined by a UV-1240 ultraviolet-visible spectrophotometer. All measurements were performed at room temperature.

3 Results and discussion

3.1 Characterizations of structure and morphology

Magnetic-luminescent bifunctional $CoFe_2O_4$@YAG:Tb^{3+} coaxial nanofibers have been successfully synthesized by electrospinning technology using a homemade coaxial spinneret. The phase compositions of $CoFe_2O_4$@YAG:7%Tb^{3+} coaxial nanofibers (S_{a3}) and $CoFe_2O_4$/YAG:7%Tb^{3+} composite nanofibers (S_{b1}) are characterized by means of XRD analysis, as shown in Figure 2. It can be seen that XRD patterns of $CoFe_2O_4$@YAG:7%Tb^{3+} coaxial nanofibers and $CoFe_2O_4$/YAG:7%Tb^{3+} composite nanofibers are respectively conformed to the cubic phase with primitive structure of YAG (PDF#33-0040) and the cubic spinel structure of $CoFe_2O_4$ (PDF#22-1086), indicating that $CoFe_2O_4$@YAG:7%Tb^{3+} coaxial nanofibers and $CoFe_2O_4$/YAG:7%Tb^{3+} composite nanofibers contain crystalline YAG:7%Tb^{3+} and $CoFe_2O_4$.

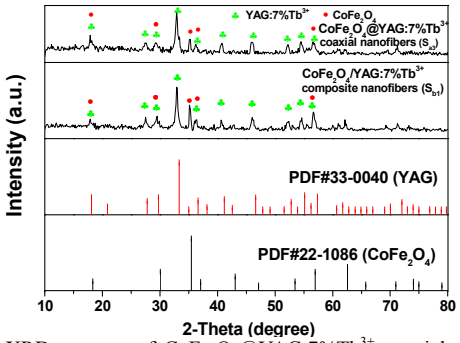

Figure 2. XRD patterns of $CoFe_2O_4$@YAG:7%Tb^{3+} coaxial nanofibers (S_{a3}) and $CoFe_2O_4$/YAG:7%Tb^{3+} composite nanofibers (S_{b1}) with PDF standard cards of YAG and $CoFe_2O_4$

Figure 3 shows morphologies of $CoFe_2O_4$ nanofibers (S), [$CoFe_2O_4$/PVP]@[$(Y(NO_3)_3$+$Tb(NO_3)_3$+$Al(NO_3)_3)$/PVP] composite coaxial nanofibers (named S_c) fabricated by the core spinning solution A1 ($CoFe_2O_4$/PVP=1:1) and the shell spinning solution B3 (Tb^{3+}/Y^{3+}=7:93) and $CoFe_2O_4$@YAG:7%Tb^{3+} coaxial nanofibers (S_{a3}), respectively. $CoFe_2O_4$ nanofibers have coarse surface and the size distribution of the as-prepared nanofibers are almost uniform, as shown in Figure 3a. It is found from Figure 3b that [$CoFe_2O_4$/PVP]@[$(Y(NO_3)_3$+$Tb(NO_3)_3$+$Al(NO_3)_3)$/PVP]

composite coaxial nanofibers are smooth. As seen from Figure 3c, the diameter of $CoFe_2O_4$@YAG:7%Tb^{3+} coaxial nanofibers is decreased owing to decomposition and volatilization of PVP and decomposition of rare earth nitrates, and the $CoFe_2O_4$@YAG:7%Tb^{3+} coaxial nanofibers have relatively coarse surface. Image-Pro Plus 6.0 software is used to measure diameters of 100 nanofibers from SEM images, and the results are analyzed with statistics, and then the histogram of diameters distribution of the nanofibers is drawn by using Origin 8.5 software. The diameters of $CoFe_2O_4$ nanofibers (S), [$CoFe_2O_4$/PVP]@[($Y(NO_3)_3$+$Tb(NO_3)_3$+$Al(NO_3)_3$)/PVP] composite coaxial nanofibers (S_c) and $CoFe_2O_4$@YAG:7%Tb^{3+} coaxial nanofibers (S_{a3}) are 77.19±10.42 nm, 749.87±19.15 nm and 293.62±34.52 nm under the confidence level of 95%, respectively, as demonstrated in Figure 4.

The TEM images of [$CoFe_2O_4$/PVP]@[($Y(NO_3)_3$+$Tb(NO_3)_3$+$Al(NO_3)_3$)/PVP] composite coaxial nanofibers (S_c), $CoFe_2O_4$@YAG:7%Tb^{3+} coaxial nanofibers (S_{a3}), $CoFe_2O_4$/[($Y(NO_3)_3$+$Tb(NO_3)_3$+$Al(NO_3)_3$)]/PVP composite nanofibers and $CoFe_2O_4$/YAG:7%Tb^{3+} composite nanofibers (S_{b1}) are respectively presented in Figure 3d, Figure 3e, Figure 3f and Figure 3g. As revealed in Figure 3d and Figure 3e, an obvious coaxial structure can be seen in the [$CoFe_2O_4$/PVP]@[($Y(NO_3)_3$+$Tb(NO_3)_3$+$Al(NO_3)_3$)/PVP] composite coaxial nanofibers and $CoFe_2O_4$@YAG:7%Tb^{3+} coaxial nanofibers, and the $CoFe_2O_4$ nanofibers are clearly observed in the core of the coaxial nanofibers. The diameters of the [$CoFe_2O_4$/PVP]@[($Y(NO_3)_3$+$Tb(NO_3)_3$+$Al(NO_3)_3$)/PVP] composite coaxial nanofibers and $CoFe_2O_4$@YAG:7%Tb^{3+} coaxial nanofibers are 700-750 nm and 270-300 nm, respectively, which are in good agreement with results of SEM analyses. It can be observed from Figure 3f and Figure 3g that $CoFe_2O_4$ nanofibers are dispersed in the $CoFe_2O_4$/[($Y(NO_3)_3$+$Tb(NO_3)_3$+$Al(NO_3)_3$)]/PVP composite nanofibers and $CoFe_2O_4$/YAG:7%Tb^{3+} composite nanofibers. From the above SEM and TEM analyses, we can confirm that the $CoFe_2O_4$@YAG:7%Tb^{3+} coaxial nanofibers have been successfully fabricated.

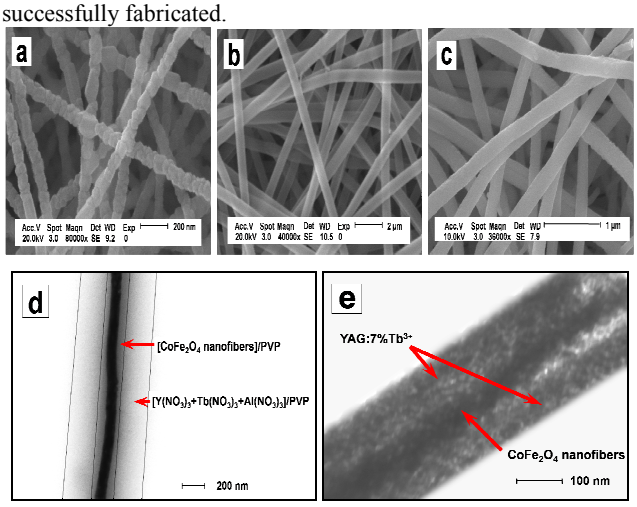

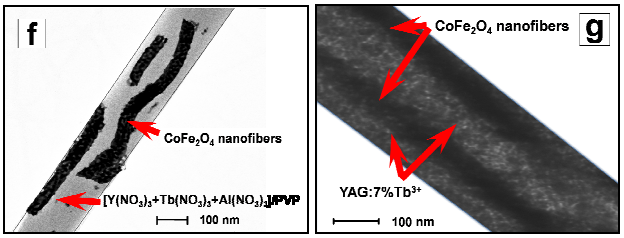

Figure 3. SEM images of $CoFe_2O_4$ nanofibers (S) (a), [$CoFe_2O_4$/PVP]@[($Y(NO_3)_3$+$Tb(NO_3)_3$+$Al(NO_3)_3$)/PVP] composite coaxial nanofibers (S_c) (b) and $CoFe_2O_4$@YAG:7%Tb^{3+} coaxial nanofibers (S_{a3}) (c), TEM images of [$CoFe_2O_4$/PVP]@[($Y(NO_3)_3$+$Tb(NO_3)_3$+$Al(NO_3)_3$)/PVP] composite coaxial nanofibers (S_c) (d), $CoFe_2O_4$@YAG:7%Tb^{3+} coaxial nanofibers (S_{a3}) (e), $CoFe_2O_4$/[($Y(NO_3)_3$+$Tb(NO_3)_3$+$Al(NO_3)_3$)]/PVP composite nanofibers (f) and $CoFe_2O_4$/YAG:7%Tb^{3+} composite nanofibers (S_{b1}) (g)

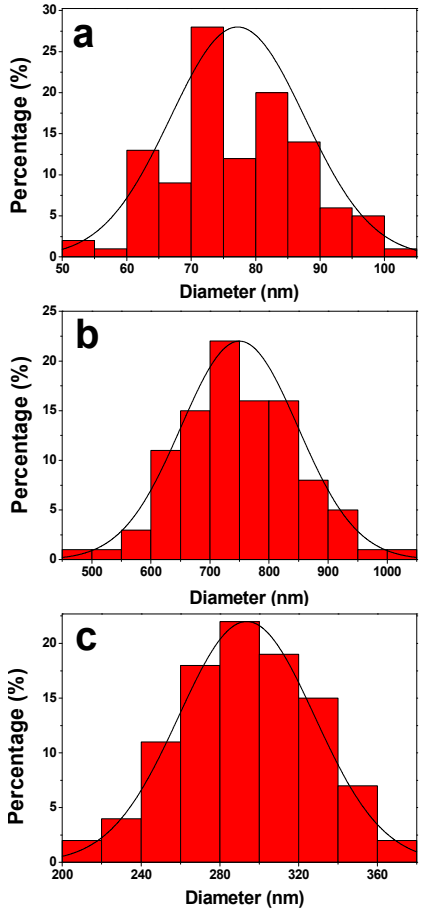

Figure 4. Histograms of diameters distribution of $CoFe_2O_4$ nanofibers (S) (a), [$CoFe_2O_4$/PVP]@[($Y(NO_3)_3$+$Tb(NO_3)_3$+$Al(NO_3)_3$)/PVP] composite coaxial nanofibers (S_c) (b) and $CoFe_2O_4$@YAG:7%Tb^{3+} coaxial nanofibers (S_{a3}) (c)

3.2 Luminescent properties of $CoFe_2O_4$@YAG:Tb^{3+} coaxial nanofibers

In order to obtain the optimum ratio of Tb^{3+} to (Tb^{3+}+Y^{3+}), a series of $CoFe_2O_4$@YAG:x%Tb^{3+} [x=1, 5, 7 and 9] coaxial nanofibers (S_{a1}, S_{a2}, S_{a3} and S_{a4}) are fabricated by coaxial electrospinning process. In order to perform this study, the mass ratio of $CoFe_2O_4$ nanofibers to PVP is fixed as 1:1 and the doping concentrations of Tb^{3+} ions vary from 1 to 9. It can be observed from Figure 5a that the excitation spectra (monitored by 544 nm) of the samples mainly consist of three bands: One strong band centering at 274 nm, and two weak bands respectively located at

230 nm and 325 nm, are attributed to transition of the ground state to the split 5d energy levels, namely $4f^8 \rightarrow 4f^7 5d$ energy levels transitions of Tb^{3+} [11, 12]. The other peaks between 340 and 500 nm, are corresponding to the intra-shell 4f-4f transitions of Tb^{3+} ions. As shown in Figure 5b, the emission spectrum under the excitation of 274-nm ultraviolet light could be separated into two groups. The blue emission below 480 nm was from $^5D_3$-^7F_J transitions while the green emission above 480 nm was from $^5D_4$-^7F_J transitions. The spectral energy distributions of Tb^{3+} emission strongly depended on the Tb^{3+} concentration[31]. The blue emission ($^5D_3$-^7F_J) dominated for very low Tb concentration (≤0.12%), it decreased with increasing Tb^{3+} concentration and nearly disappeared for Tb^{3+} concentration above 1%, and then the green emission ($^5D_4$-^7F_J) started to dominate, as shown in the Figure 5b. This result was in good agreement with the references[10-13]. With the Tb^{3+} concentration increasing, the cross relaxation from $^5D_3$ level to $^5D_4$ level leaded to a strong emission in the green region. The characteristic emission peaks of Tb^{3+} are observed and ascribed to the energy levels transitions of $^5D_4 \rightarrow {}^5F_6$ (489 nm), $^5D_4 \rightarrow {}^5F_5$ (544 nm), $^7D_4 \rightarrow {}^5F_4$ (587 nm) and $^5D_4 \rightarrow {}^7F_3$ (623 nm) of Tb^{3+} ions, and the $^5D_4 \rightarrow {}^5F_5$ energy levels transition at 544 nm is the predominant emission peak. It is found from Figure 5 that the spectral shape and locations of excitation and emission peaks do not remarkably vary with the increase of the doping concentrations of Tb^{3+} ions for $CoFe_2O_4$@YAG:x%Tb^{3+} [x=1, 5, 7 and 9] coaxial nanofibers, but the intensity of excitation and emission peaks for $CoFe_2O_4$@YAG:Tb^{3+} coaxial nanofibers strongly depend on the doping concentration of Tb^{3+} ions, and the strongest excitation and emission spectra can be obtained when the doping molar concentration of Tb^{3+} is 7%.

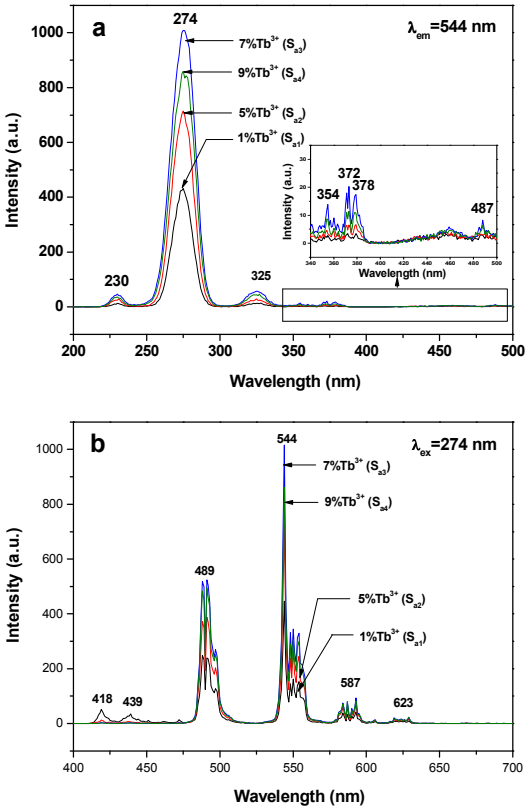

Figure 5. Excitation spectra (a) and emission spectra (b) of $CoFe_2O_4$@YAG:x%Tb^{3+} [x=1, 5, 7 and 9] coaxial nanofibers (S_{a1}, S_{a2}, S_{a3} and S_{a4}) when the mass ratio of $CoFe_2O_4$ nanofibers to PVP is fixed at 1:1

3.3 CIE analysis

Generally, color can be represented by the Commission Internationale de L'Eclairage (CIE) 1931 chromaticity coordinates. The chromaticity coordinates and color ratios have been calculated from the emission spectra by the method described in previous report[33]. The emission colors of $CoFe_2O_4$@YAG:x%Tb^{3+} [x=1, 5, 7 and 9] coaxial nanofibers (S_{a1}, S_{a2}, S_{a3} and S_{a4}) appear in the green region, as indicated in Figure 6. The chromaticity coordinates (X, Y) of $CoFe_2O_4$@YAG:Tb^{3+} coaxial nanofibers excited by 274 nm are (0.2464, 0.4818), (0.2517, 0.5092), (0.2619, 0.5525) and (0.2620, 0.5666), which correspond to $CoFe_2O_4$@YAG:x%Tb^{3+} [x=1, 5, 7 and 9] coaxial nanofibers, respectively. It can be seen that the chromaticity coordinates change with the increase of Tb^{3+} concentration s. According to the above results, it can be found that the emission colors of $CoFe_2O_4$@YAG:Tb^{3+} coaxial nanofibers can be tuned by adjusting the concentrations of Tb^{3+} ions, which are considered to be promising candidates for application in LEDs.

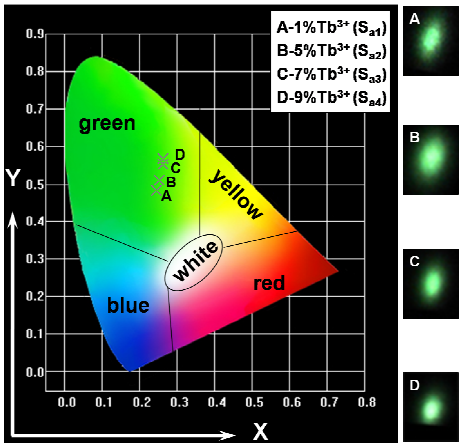

Figure 6. CIE chromaticity coordinates diagram of $CoFe_2O_4$@YAG:x%Tb^{3+} [x=1, 5, 7 and 9] coaxial nanofibers (S_{a1}, S_{a2}, S_{a3} and S_{a4})

The excitation spectra (monitored at 544 nm) and emission spectra (excited by 274 nm) of $CoFe_2O_4$@YAG:Tb^{3+} coaxial nanofibers (S_{a3}, S_{a5} and S_{a6}) containing different amounts of $CoFe_2O_4$ magnetic nanofibers are indicated in Figure 7. In order to perform this investigation, the doping concentration of Tb^{3+} ions is fixed at 7% and the mass ratios of $CoFe_2O_4$ nanofibers to PVP are varied from 1:1 to 1:5. As seen from Figure 7, the excitation and emission intensity of $CoFe_2O_4$@YAG:7%Tb^{3+} coaxial nanofibers (S_{a3}, S_{a5} and S_{a6}) do not remarkably change with the increase of the amount of $CoFe_2O_4$ nanofibers introduced into the coaxial nanofibers. A YAG:Tb^{3+} nanofiber is divided into three imaginary parts by dash lines. Large quantities of luminescence centers (YAG:Tb^{3+}) are dispersed in the nanofiber. The exciting light would get weak due to the light absorption of the components of the fiber when it reached the core part and emitted weak emitting light. Meanwhile, the weak emitting light could barely pass through the components of the fiber to reach the external of the fiber. Only the luminescence centers dispersed in the middle and surface parts contribute to the luminescence intensity of the fiber. As a result, the core domain of the fiber could be displaced by magnetic core ($CoFe_2O_4$) and almost do not affect the luminescence performance of the fiber.

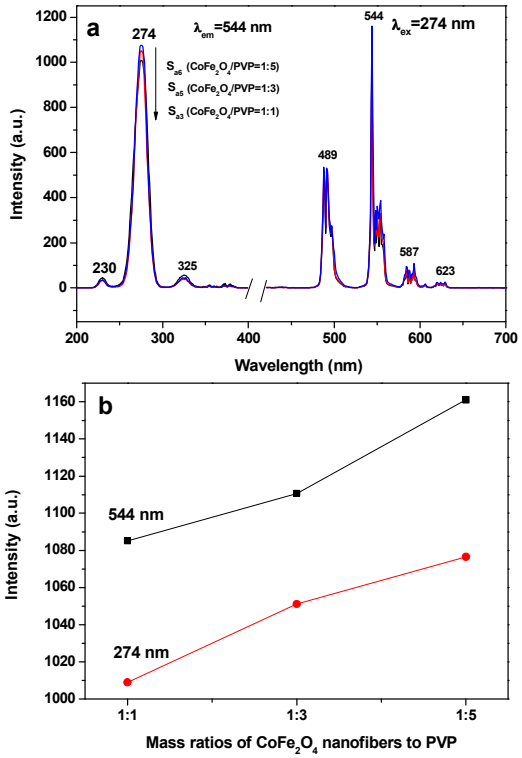

Figure 7. Excitation and emission spectra (a) of $CoFe_2O_4$@YAG:7%Tb^{3+} coaxial nanofibers (S_{a3}, S_{a5} and S_{a6}) containing different mass ratios of $CoFe_2O_4$ nanofibers to PVP and dependence of excitation peak intensity (at 274 nm) and emission peak intensity (at 544 nm) on mass ratios of $CoFe_2O_4$ nanofibers to PVP for $CoFe_2O_4$@YAG:7%Tb^{3+} coaxial nanofibers (b)

From the ultraviolet-visible diffuse reflectance spectrum of $CoFe_2O_4$ nanofibers illustrated in Figure 8, it is observed that $CoFe_2O_4$ nanofibers can absorb light at ultraviolet wavelengths (<400 nm) much more strongly than visible range (400-700 nm). Both the exciting light (274 nm) and emitting light (489-623 nm) can be absorbed by dark-colored $CoFe_2O_4$.

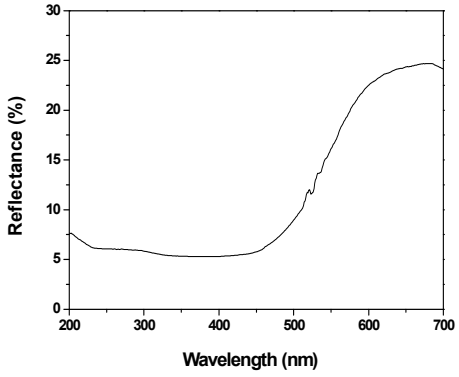

Figure 8. UV-vis diffuse reflectance spectrum of $CoFe_2O_4$ nanofibers

To illustrate the advantages of the nanostructure of the magnetic-luminescent bifunctional coaxial nanofibers, the $CoFe_2O_4$/YAG:7%Tb^{3+} composite nanofibers (S_{b1}), as a contrast sample, were also fabricated by mixing the core spinning solution A1 ($CoFe_2O_4$/PVP=1:1) and the shell spinning solution B3 (Tb^{3+}/Y^{3+}=7:93) together followed by electrospinning via the traditional single-spinneret electrospinning setup. From the contrast between the $CoFe_2O_4$@YAG:7%Tb^{3+} coaxial nanofibers (S_{a3}) and $CoFe_2O_4$/YAG:7%Tb^{3+} composite nanofibers (S_{b1}) which have the same components, as shown in Figure 9. The excitation and emission intensity of coaxial nanofibers are much stronger than those of composite nanofibers, and this weak luminescent emission intensity makes the composite nanofibers impractical in luminescent performance.

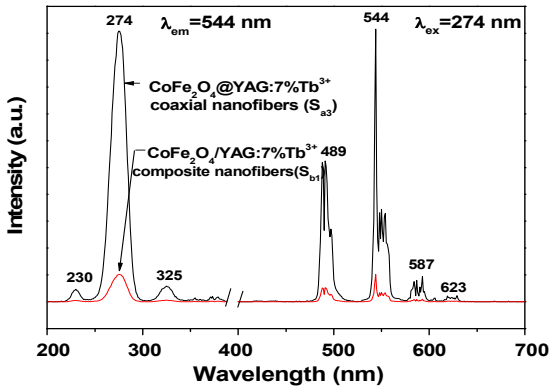

Figure 9. Excitation and emission spectra of $CoFe_2O_4$@YAG:7%Tb^{3+} coaxial nanofibers (S_{a3}) and $CoFe_2O_4$/YAG:7%Tb^{3+} composite nanofibers (S_{b1})

As illustrated in Figure 10, $CoFe_2O_4$ nanofibers are promiscuously dispersed in the $CoFe_2O_4$/YAG:7%Tb^{3+} composite nanofiber. The exciting light in the composite nanofiber has to pass through $CoFe_2O_4$ nanofibers to reach and excite YAG:7%Tb^{3+} luminescence center. In this process, a large part of the exciting light has been absorbed by $CoFe_2O_4$ nanofibers, and thus the exciting light is much weakened before it reaches the YAG:7%Tb^{3+} center. Similarly, the light emitted by YAG:7%Tb^{3+} luminescence center also has to pass through $CoFe_2O_4$ nanofibers and is absorbed by them. Consequently, both the exciting and emitting light are severely weakened. For the $CoFe_2O_4$@YAG:7%Tb^{3+} coaxial nanofibers, the $CoFe_2O_4$ nanofibers only disperse in the core of the coaxial nanofibers so that the exciting light and emitting light will be little affected by $CoFe_2O_4$ nanofibers. The overall effect is that the $CoFe_2O_4$@YAG:7%Tb^{3+} coaxial nanofibers possess much higher luminescent performance than the $CoFe_2O_4$/YAG:7%Tb^{3+} composite nanofibers.

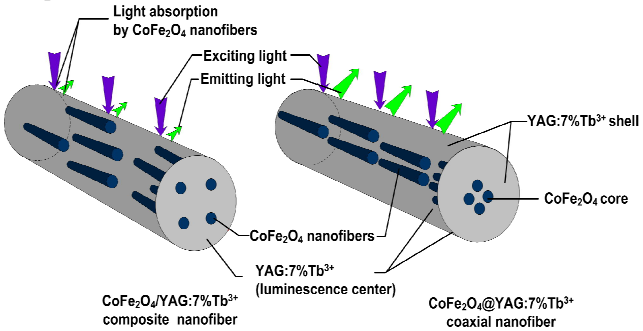

Figure 10. Schematic diagram of the situation of the exciting light and emitting light in $CoFe_2O_4$/YAG:7%Tb^{3+} composite nanofiber and $CoFe_2O_4$@YAG:7%Tb^{3+} coaxial nanofiber

The excitation and emission spectra of $CoFe_2O_4$@YAG:7%Tb^{3+} coaxial nanofibers (S_{a3}) after three cycles of magnetization are presented in Figure 11. As illustrated in Figure 11a and Figure 11b, the excitation and emission intensity of $CoFe_2O_4$@YAG:7%Tb^{3+} coaxial nanofibers do not remarkably change after three cycles of magnetization, demonstrating that the novel coaxial nanofibers still have good luminescent performance after three magnetic measurements.

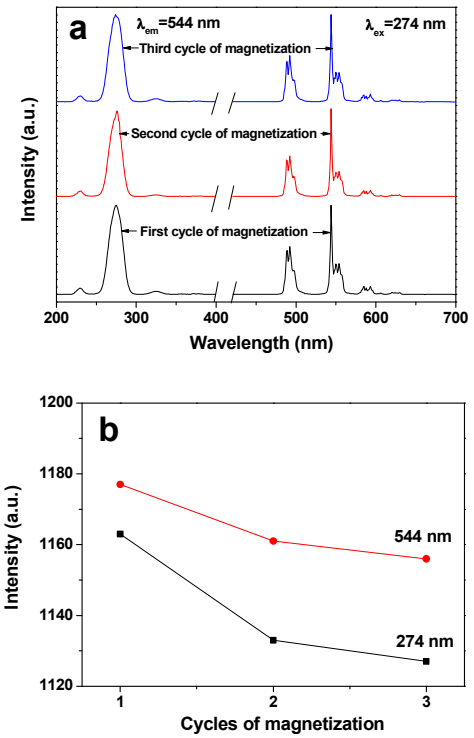

Figure 11. Excitation and emission spectra (a) of $CoFe_2O_4$@YAG:7%Tb^{3+} coaxial nanofibers (S_{a3}) after three cycles of magnetization and dependence of excitation peak intensity (at 274 nm) and emission peak intensity (at 544 nm) on cycles of magnetization for $CoFe_2O_4$@YAG:7%Tb^{3+} coaxial nanofibers (b)

3.4 Magnetic properties of $CoFe_2O_4$@YAG:Tb^{3+} coaxial nanofibers

The typical hysteresis loops for $CoFe_2O_4$ nanofibers (S), $CoFe_2O_4$@YAG:7%Tb^{3+} coaxial nanofibers (S_{a3}, S_{a5} and S_{a6}) and $CoFe_2O_4$/YAG:7%Tb^{3+} composite nanofibers (S_{b1}) are shown in Figure 12, and the saturation magnetizations, coercivity and remanence of them are listed in Table 2. As seen from Figure 12, the saturation magnetization of the $CoFe_2O_4$ nanofibers is 45.80 emu·g^{-1}, which is similar to the data reported by previous literatures[14-17]. The saturation magnetization of $CoFe_2O_4$@YAG:7%Tb^{3+} coaxial nanofibers containing different mass ratios of $CoFe_2O_4$ nanofibers to PVP are 21.70 emu·g^{-1}, 6.21 emu·g^{-1} and 3.65 emu·g^{-1}, respectively, as revealed in Figure 12 and Table 2. It is known that the saturation magnetization of a magnetic composite material depends on the mass percentage of the magnetic substance in the magnetic composite material[23-25]. It is found that the saturation magnetization of the $CoFe_2O_4$@YAG:7%Tb^{3+} coaxial nanofibers is increased with the increase in the amount of $CoFe_2O_4$ magnetic nanofibers introduced into the core of the coaxial nanofibers, implying that the magnetism of the coaxial nanofibers can be tunable by adjusting the amount of $CoFe_2O_4$ magnetic nanofibers. The saturation magnetization of the $CoFe_2O_4$/YAG:7%Tb^{3+} composite nanofibers is 22.34 emu·g^{-1}, which is close to that of the coaxial nanofibers marked c (21.70 emu·g^{-1}) in Figure 12. Combined luminescence with magnetism analysis, it is found that when the coaxial nanofibers have the close magnetic property to the $CoFe_2O_4$/YAG:7%Tb^{3+} composite nanofibers, the luminescent intensity of the coaxial nanofibers is much higher than that of the composite nanofibers, demonstrating that the novel coaxial nanofibers have better magnetic-luminescent performance than the composite nanofibers. Based on the above experimental results, we can safely conclude that our academic ideas described in the introduction are successfully realized via coaxial electrospinning.

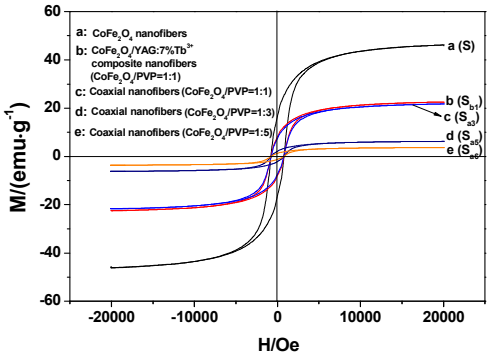

Figure 12. Hysteresis loops of $CoFe_2O_4$ nanofibers (S) (a), $CoFe_2O_4$/YAG:7%Tb^{3+} composite nanofibers (S_{b1}) (b) and $CoFe_2O_4$@YAG:7%Tb^{3+} coaxial nanofibers (S_{a3}, S_{a5} and S_{a6}) containing different mass ratios of $CoFe_2O_4$ nanofibers to PVP (c, d, e)

Table 2. Saturation magnetization, coercivity and remanence of samples

Samples	Saturation magnetization (Ms)/(emu·g^{-1})	Coercivity (Hc)/(Oe)	Remanence (Br)/(emu·g^{-1})
$CoFe_2O_4$ nanofibers (S)	45.80	785	16.49
Composite nanofibers S_{b1} ($CoFe_2O_4$/PVP=1:1)	22.34	763	7.49
Coaxial nanofibers S_{a3} ($CoFe_2O_4$/PVP=1:1)	21.70	759	7.11
Coaxial nanofibers S_{a5} ($CoFe_2O_4$/PVP=1:3)	6.21	743	2.56
Coaxial nanofibers S_{a6} ($CoFe_2O_4$/PVP=1:5)	3.65	735	1.40

4 Conclusions

In summary, magnetic-luminescent bifunctional $CoFe_2O_4$@YAG:7%Tb^{3+} coaxial nanofibers have been successfully synthesized by electrospinning technology using a homemade coaxial spinneret. It is very gratifying to see that the magnetic-luminescent bifunctional coaxial nanofibers simultaneously possess excellent luminescent performance and magnetic properties. Furthermore, the luminescent intensity, color and saturation magnetization of the coaxial nanofibers can be tuned via adjusting the concentrations of rare earth ions and the amount of $CoFe_2O_4$ magnetic nanofibers. $CoFe_2O_4$@YAG:7%Tb^{3+} magnetic-luminescent bifunctional coaxial nanofibers prepared are low toxicity. The MRI and ultraviolet image can be obtained under applied magnetic field and ultraviolet light, respectively. The new high-performance coaxial nanofibers can serve as both magnetic resonance contrast agents for MRI and optical probes for luminescence imaging techniques, which provide complementary information in cellular

monitoring. It would either allow for external manipulation of the carrier with a magnetic field and real time visualization with luminescence imaging techniques, or use of the carrier for magnetic separation followed by luminescent detection. Besides, other multifunctional nanomaterials can be designed and fabricated based on this novel design conception and construct technology.

Acknowledgements

This work was financially supported by the National Natural Science Foundation of China (NSFC 50972020, 51072026), Specialized Research Fund for the Doctoral Program of Higher Education (20102216110002, 20112216120003), the Science and Technology Development Planning Project of Jilin Province (Grant Nos. 20130101001JC, 20070402), the Science and Technology Research Project of the Education Department of Jilin Province during the eleventh five-year plan period (Under grant No. 2010JYT01).

Notes and references

Key Laboratory of Applied Chemistry and Nanotechnology at Universities of Jilin Province, Changchun University of Science and Technology, Changchun, China. Fax: +86-0431-85383815; Tel: +86-0431-85582574; E-mail: dongxiangting888@163.com

1. W. Wang, Z.Y. Li, X.R. Xu, B. Dong, H.N. Zhang, Z.J. Wang, C. Wang, R.H. Baughman, S.L. Fang, *Small*, 2011, **7**, 597-600.
2. J. Feng, S.Y. Song, R.P. Deng, W.Q. Fan, H.J. Zhang, *Langmuir*, 2010, **26**, 3596-3600.
3. H.Y. Chen, D. C. Colvin, B. Qi, T. Moore, J. He, O.T. Mefford, Fr. Alexis, J.C. Gore, J.N. Anker, *J. Mater. Chem.*, 2012, **22**, 12802-12809.
4. P. Lu, J.L. Zhang, Y.L. Liu, D.H. Sun, G.X. Liu, G.Y. Hong, J.Z. Ni, *Talanta*, 2010, **83**, 450-457.
5. W. Wang, M. Zou, K.Z. Chen, *Chem. Commun.*, 2010, **46**, 5100-5102.
6. C. Goubault, P. Jop, M. Fermigier, J. Baudry, E. Bertrand, J. Bibette, *Phys. Rev. Lett.*, 2003, **91**, 260802.
7. H.G. Wang, L. Sun, Y.P. Li, X.L. Fei, M.D. Sun, C.Q. Zhang, Y.X. Li, Q.B. Yang, *Langmuir*, 2011, **27**, 11609-11615.
8. P. Sun, H.Y. Zhang, C. Liu, J. Fang, M. Wang, J. Chen, J.P. Zhang, C.B. Mao, S.K. Xu, *Langmuir*, 2010, **26**, 1278-1284.
9. F. Grasset, F. Dorson, Y. Molard, S. Cordier, V. Demange, C. Perrin, V. M. Artzner, H. Haneda, *Chem. Commun.*, 2008, **39**, 4729-4731.
10. L.N. Chen, J. Wang, W.T. Li, H.Y. Han, *Chem. Commun.*, 2012, **48**, 4971-4973.
11. A. Potdevin, G. Chadeyron, V. Briois, F. Lerouxb, R. Mahiou, *Dalton Trans.*, 2010, **39**, 8718-8724.
12. K. Guo, M.L. Huang, H.H. Chen, X.X. Yang, J.T. Zhao, *J. Non-Cryst. Solids*, 2012, **358**, 88-92.
13. X. Li, H. Liu, J.Y. Wang, H.M. Cui, S.L. Yang, I.R. Boughton, *J. Phys. Chem. Solids*, 2005, **66**, 201-205.
14. R. Kubrin, W. Bauhofer, *Mater. Sci. Eng.: B*, 2012, **177**, 1605-1611.
15. J.C. Fu, J.L. Zhang, Y. Peng, J.G. Zhao, G.G. Tan, N. J. Mellors, E.Q. Xie, Weihua Han, *Nanoscale*, 2012, **4**, 3932-3936.
16. A. Kovalenko, J. Jouhannaud, P. Polavarapu, M.P. Krafft, G. Watona, G. Pourroy, *Soft Matter*, 2014, **10**, 5147-5156.
17. I. Andreu, E. Natividad, C. Ravagli, M. Castro, G.i Baldi, *RSC Adv.*, 2014, **4**, 28968-28977.
18. R.L. Ji, C.B. Cao, Z. Chen, H.Z. Zhai, J. Bai, *J. Mater. Chem. C.*, 2014, **2**, 5944-5953.
19. Z.Y. Hou, C.X. Li, P.G. Ma, G.G. Li, Z.Y. Cheng, C. Peng, D.M. Yang, P.P. Yang, J. Lin, *Adv. Funct. Mater.*, 2011, **21**, 2356-2365.
20. J.S. McLane, N.J. Schaub, R.J. Gilbert, L.A. Ligon, *Methods Mol. Biol.*, 2013, **1046**, 371-388.
21. X.F. Lu, C. Wang, Y, Wei, *Small*, 2009, **5**, 2349-2370.
22. J.B. Mu, C.L. Shao, Z.C. Guo, Z.Y. Zhang, M.Y. Zhang, P. Zhang, B. Chen, Y.C. Liu, *Appl. Mater. Interfaces*, 2011, **3**, 590-596.
23. W. Sambaer, M. Zatloukal, D. Kimmer, *Chem. Eng. Sci.*, 2011, **66**, 613-623.
24. S.L. Chen, H.Q. Hou, F. Harnisch, S.A. Patil, A.A.C. Martinez, S. Agarwal, Y.Y. Zhang, S.S. Ray, A.L. Yarin, A. Greiner, U. Schröder, *Energy Environ. Sci.*, 2011, **4**, 1417-1421.
25. J. Song, M.L. Chen, M.B. Olesen, C.X. Wang, R. Havelund, Q. Li, E.Q. Xie, R. Yang, P. Bøggild, C. Wang, F. Besenbacher, M.D. Dong, *Nanoscale*, 2011, **3**, 4966-4971.
26. Y. Ma, H. Li, L. Wang, *J. Mater. Chem.,* 2012, **22**, 18761-18767.
27. H. Wang, Y. Li, L. Sun, Y. Li, W. Wang, S. Wang, S. Xu, Q. Yang, J. *Colloid Interface Sci.,* 2010, **350**, 396-401.
28. Q.L. Ma, W.S. Yu, X.T. Dong, J.X. Wang, G.X. Liu, *Nanoscale*, 2014, **6**, 2945-2952.
29. Q.L. Ma, J.X. Wang, X.T. Dong, W.S. Yu, G.X. Liu, *ChemPlusChem*, 2014, **79**, 290-297.
30. X. Xi, J.X. Wang, X.T. Dong, Q.L. Ma, W.S. Yu, G.X. Liu, *Chem. Eng. J.*, 2014, **254**, 259-267.
31. Q.L. Ma, J.X. Wang, X.T. Dong, W.S. Yu, G.X. Liu, J. Xu, *J. Mater. Chem.*, 2012, **22**, 14438-14442.
32. D.J. Robbins, B. Cockayne, B. Lent, J.L. Glasper, *Solid State Commun.*, 1976, **20**, 673-676.
33. Z.F. Zhu, D.G. Liu, H. Liu, G.J. Li, J. Du, Z.L. He, *J. Lumin.,* 2012, **132**, 261-265.